A THREE-DIMENSIONAL CLOUD-SCALE MODEL SUITABLE FOR COMPRESSIBLE ATMOSPHERE

Xu Huanbin (许焕斌) and *Wang Siwei* (王思微)

Academy of Meteorological Science, State Meteorological Administration, Beijing

Received February 3, 1990

ABSTRACT

A three-dimensional cloud-scale model has been designed. The governing equations of the model are composed of two groups of equations: one group includes compressible motion equations, continuity equation, pressure equation and thermodynamic equation, which are of Eulerian type, and the other consists of cloud-precipitation microphysics equations which are of Lagrangian type. Since the degree of influence of sound wave on the air motion is quite different from that on the temperature or hydrometeors, the time splitting procedure is used in solving governing equations. Both unstaggered and staggered meshes have been utilized. Integration schemes adopted are the Eulerian backward difference method for the unstaggered mesh and semi-implicit method for staggered mesh. Several experiments of modelling have been conducted and a reasonable three-dimensional image of deep convection is obtained. With this model the horizontal and vertical vortex circulations are simulated. Furthermore, the effects of horizontal vortex on the formation and development of downdraft within cloud have also been studied.

I. INTRODUCTION

It is well known that many atmospheric phenomena are three dimensional and the supercell storm is a typical one which attracts meteorologists' attention. Several numerical models have been designed by Schlesinger (1978), Klemp and Wilhelson (1978), Tripoli and Cotton (1982) , etc. In addition, some mesoscale models have achieved considerable success through introducing detailed physical processes and the fine mesh of large-scale numerical model (Anthes & Warner,1978; Zhou, 1980; Chen, 1980).However this kind of model is suitable only for meso-α weather system because its governing equations are quasi-static. Since the strongest mesoscale system is often convective system or convective complex of meso-β scale with several convective circulations included which are meso-γ scale or intermediate between the meso-β and meso-γ scales, it is necessary to develop a model in which governing equations are complete, cloud physical processes are appropriate and the interactions between different scales are considered. The anelastic approximation adopts a balanced and elliptic equation with prognostic nature eliminated, therefore utilization of compressible motion and continuity equations has more flexibilities and wide applications to severe convective phenomena with various scales and different intensities. As the first step, we have used the compressible equations and designed a three-dimensional cloud-scale model in which the governing equations are not simplified as far as possible, the scheme of treatment for microphysical processes is alternative, and the interaction between hydrometeor and convective airflow fields is considered particularly.

II. THE DESCRIPTION OF THE MODEL

The equations of the model are composed of both Eulerian and Lagrangian type

equations. The equations of motion, continuity and pressure belong to the former and the cloud-precipitation microphysical equations to the latter. This model may have advantage to improve the interaction between hydrometeor and airflow fields within cloud bodies.

Let

$$P(x,y,z,t)=P_0(z)+P'(x,y,z,t),$$
$$\rho(x,y,z,t)=\rho_0(z)+\rho'(x,y,z,t),$$
$$T_v(x,y,z,t)=T_{v0}(z)+T_v'(x,y,z,t).$$

1. *Eulerian Type Basic Equations*

(1) Equation of state

$$P=\rho RT_v. \tag{1}$$

(2) Equations of motion

$$\frac{\partial u}{\partial t}=-u\frac{\partial u}{\partial x}-v\frac{\partial u}{\partial y}-w\frac{\partial u}{\partial z}-\frac{1}{\rho_0}\frac{\partial P'}{\partial x}+K\nabla^2u, \tag{2}$$

$$\frac{\partial v}{\partial t}=-u\frac{\partial v}{\partial x}-v\frac{\partial v}{\partial y}-w\frac{\partial v}{\partial z}-\frac{1}{\rho_0}\frac{\partial P'}{\partial y}+K\nabla^2v, \tag{3}$$

$$\frac{\partial w}{\partial t}=-u\frac{\partial w}{\partial x}-v\frac{\partial w}{\partial y}-w\frac{\partial w}{\partial z}-\frac{1}{\rho_0}\frac{\partial P'}{\partial z}+K\nabla^2w+g\left(\frac{T_v'}{T_{v0}}-\frac{\tau}{\rho_0}-\frac{P'}{P_0}\right). \tag{4}$$

(3) Continuity equation

$$\frac{\partial \rho}{\partial t}+\frac{\partial \rho u}{\partial x}+\frac{\partial \rho v}{\partial y}+\frac{\partial \rho w}{\partial z}=0. \tag{5}$$

(4) Thermodynamic equation

$$\frac{\partial T}{\partial t}=-u\frac{\partial T}{\partial x}-u\frac{\partial T}{\partial y}-w\frac{\partial T}{\partial z}-w\Gamma_a+\frac{1}{\rho_0C_p}\frac{dP'}{dt}+P_T/\rho_0+K\nabla^2T. \tag{6}$$

(5) Vapour continuity equation

$$\frac{\partial Q}{\partial t}=-u\frac{\partial Q}{\partial x}-v\frac{\partial Q}{\partial y}-w\frac{\partial Q}{\partial z}+P_Q/\rho_0+K\nabla^2T. \tag{7}$$

(6) Pressure change equation

$$\frac{\partial P'}{\partial t}=\bar{C}^2\frac{\rho_0}{\tau}\left(\frac{\partial u}{\partial x}+\frac{\partial v}{\partial y}+\frac{\partial w}{\partial z}\right)=f_P, \tag{8}$$

$$f_p=-\left(u\frac{\partial P'}{\partial x}+v\frac{\partial P'}{\partial y}+w\frac{\partial P'}{\partial z}\right)-P'\left(\frac{\partial u}{\partial x}+\frac{\partial v}{\partial y}+\frac{\partial w}{\partial z}\right)+\left(\frac{\bar{C}^2}{\gamma}\frac{\rho_0}{T_{v0}}+\frac{P'}{T_{v0}}\right)\frac{dT_v}{\partial t}. \tag{9}$$

They are obtained by use of Eqs. (1—5).

In the above equations Γ_a is dry adiabatic lapse rate, $\gamma=C_P/C_V$, P_T is the temperature change rate due to phase change of water vapour per unit volume of air, P_Q is the water vapour content change rate in unit volume due to sources and sinks, τ is the specific content of hydrometeor, K is exchange coefficient, and other symbols are conventional meanings in meteorological use.

The above equations are basic equations for compressible atmosphere and the computation to solve them is very time consuming. In order to suit our computer, we have simplified some physical processes such as the effects of subgrid turbulence.

2. *Lagrangian Type Cloud-Precipitation Microphysics Equations*

Unlike the fields of airflow, temperature and vapour, the hydrometeor field is not continuous and there are interfaces outside which the hydrometeor content is zero. Therefore we have some troubles with the interface when the Eulerian type microphysical equations are used on, for example, pseudo-diffusion and blurred boundary of clouds. An experiment by use of Lagrangian type equations

$$dA/dZ = P_A/\rho \tag{10}$$

is made, where A can be W_R, R, A_I or A_{NI}, which denote specific contents of cloud water, rain water and ice, and number concentration of participation particles of ice phase, respectively. The meanings of A, P_A and their expressions see the reference (Xu, 1985b). In the determination of size-distribution of raindrops and hailstones the biparameter evolution scheme is adopted (Xu, 1985a). In order to suit the numerical integration a semi-Lagrangian approach is introduced (Bates, 1982). The difference in integration between the semi-Lagrangian and the Lagrangian schemes is that the former follows a fixed air parcel only in one step-time, but the latter follows the air parcel all the time of computation. In the subroutine, first, we compute the forcing terms at a point of grid (PG), then find a point (PA) in the mesh from which the air parcel will move to PG and finally, compute the value at P_A by interpolation which is used to replace the value at PG.

III. NUMERICAL INTEGRATION OF EQUATIONS

1. *Domain of Computation*

The computation domain is $20 \times 20 \times 12.5$ km, grid length $\Delta x = 500$m, and I, J and K are horizontal and vertical grid indices, respectively. The vertical extension of the domain is not enough for deep convective activity. In order to avoid the impulse of strong updraft at the top of the domain the lapse rate of temperature is set to be absolutely stable at four points beneath the top.

2. *Grid Mesh Structure*

Two types of grid mesh schemes have been adopted: one is a spatially staggered grid referred to as GR1 and the other is unstaggered as GR2 (see Fig. 1).

3. *Finite-Difference Structure*

For GR2 the Euler's backward difference scheme is used for time integration, upstream difference for advection terms, and centered difference of second order for other spatial difference. For GR1, centered difference of fourth order is used for spatial difference and the time difference scheme is second-order leapfrog.

4. *Boundary Conditions*

For an arbitrary variable F, at the upper boundary set $\left.\frac{\partial F}{\partial z}\right|_{z=z_{top}} = 0$ and at the low boundary set $F\big|_{z=0} = 0$. For precipitation $\left.\frac{\partial F}{\partial z}\right|_{z=0} = 0$.

The lateral boundary condition is a suspending one (Xu, 1989), which has improved the influence of boundary on the airflow within computation domain.

5. *Initial Conditions*

The initial fields of T, P, Q, u, v, and w are as follows:

$$T=T_0(z),\quad P=P_0(z),\quad Q=Q_0(z),\quad v=0,\quad w=0,\quad \text{and}$$
$$u=-u_0\sin(0.5\pi K/K_0),$$

where $K_0=12$ and $u_0=600.0$cm/s. The start-up of model is triggered by the disturbance of temperature set by $T'=\Delta T \sin(0.5\pi I/I_0)\cdot\sin(0.5\pi J/J_0)$ with $\Delta T=1.5°$C, and $I_0=J_0=15$.

6. *Integration Scheme*

In the time integration of governing equations the time splitting procedure is used for both GR1 and GR2, the long time step is adopted for T, Q and A; and the short time step for u, v, w and P' which are obtained by the semi-implicit method for GR1. The long time step $\Delta T_L=8$s and the short one $\Delta T_S=0.1\ \Delta T_L=0.8$s. The integration for the long time step runs once every 10 integrations of short time step.

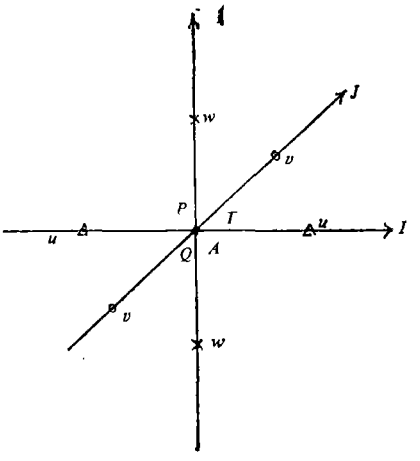

Fig. 1. The three-dimensional staggered grid arrangement. (•: P', T, A, Q; Δ: u; ⊙: v; ×: w)

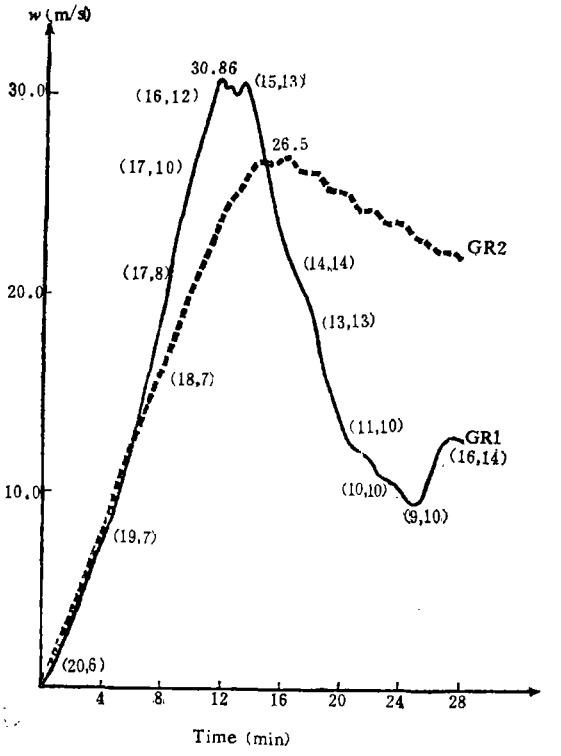

Fig. 2. The history of maximum vertical velocity w(m/s) and occurrence coordinates (I, 20, K).

IV. SIMULATION RESULTS AND CASE STUDY

Four cases have been computed by use of computer MW-1. The CPU time is 16 hours

for GR1 and 10 hours for GR2. In view of saving CPU time the GR2 is better than GR1.

1. *The Whole Verification of Model*

In order to examine the whole reliability of the model we have drawn Fig. 2, which shows the variation of maximum vertical velocity and occurrence coordinates versus time within the computation domain. From Fig. 2 we can see that the variation is continuous and reasonable. It means the dynamic framework schemes are appropriate but we have to notice that although the equations and initial-boundary conditions are same for GR1 and GR2, the variation are quite different from each other. This may be caused by different intgration schemes.

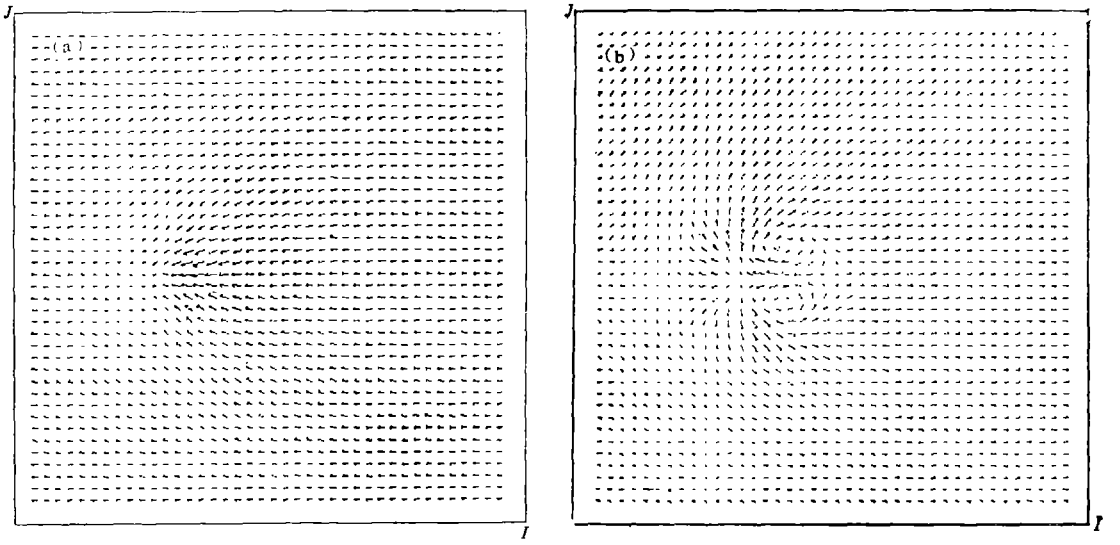

Fig. 3. The horizontal airflow field in *I-J* (*u-v*) section at $z=2.5$ (a) and 6.5km (b) (16th min).

2. *Case Study——The Formation of Horizontal Vortex and Its Effect on the Development of Downdraft*

It is well known that the severe convective cloud can produce various weather phenomena such as hail, heavy rain, gust, downburst etc. But which one occurs usually depends on the existence of associated airflow pattern. For example, the strong hailstorm is closely related to the formation of supercell airflow pattern. However the formation of this airflow pattern is not directly dependent on the development of updraft but on the genesis of strong downdraft in a cloud under appropriate conditions. We have discussed this question by using two-branch one-dimensional model and two-dimensional model, and indicated that a mid-level dry and cold airflow intruding advectively into clouds is very important for the formation and maintenance of supercell's airflow pattern (Xu and Wang, 1986, 1989). But there are some limitations for this study because the one/two-dimensional model can not describe the horizontal vortex circulation, in turn, can not study the effect of horizontal vortex. As a result, we have to use the present model which is able to simulate both horizontal and vertical vortices.

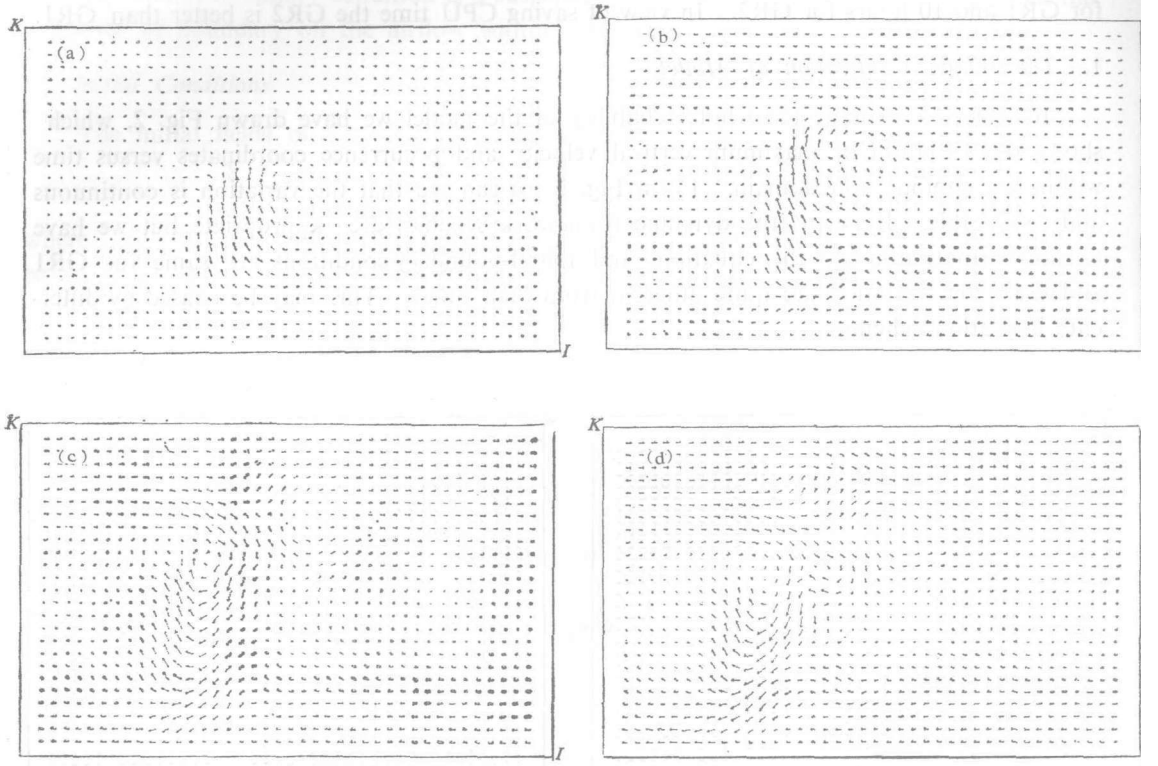

Fig. 4. The vertical airflow field in *I-K* section (*u-w* vector) at $J=20$ and for 12—24 min. (a) $T=12$min; (b) $T=16$min; (c) $T=20$min; and (d) $T=24$min.

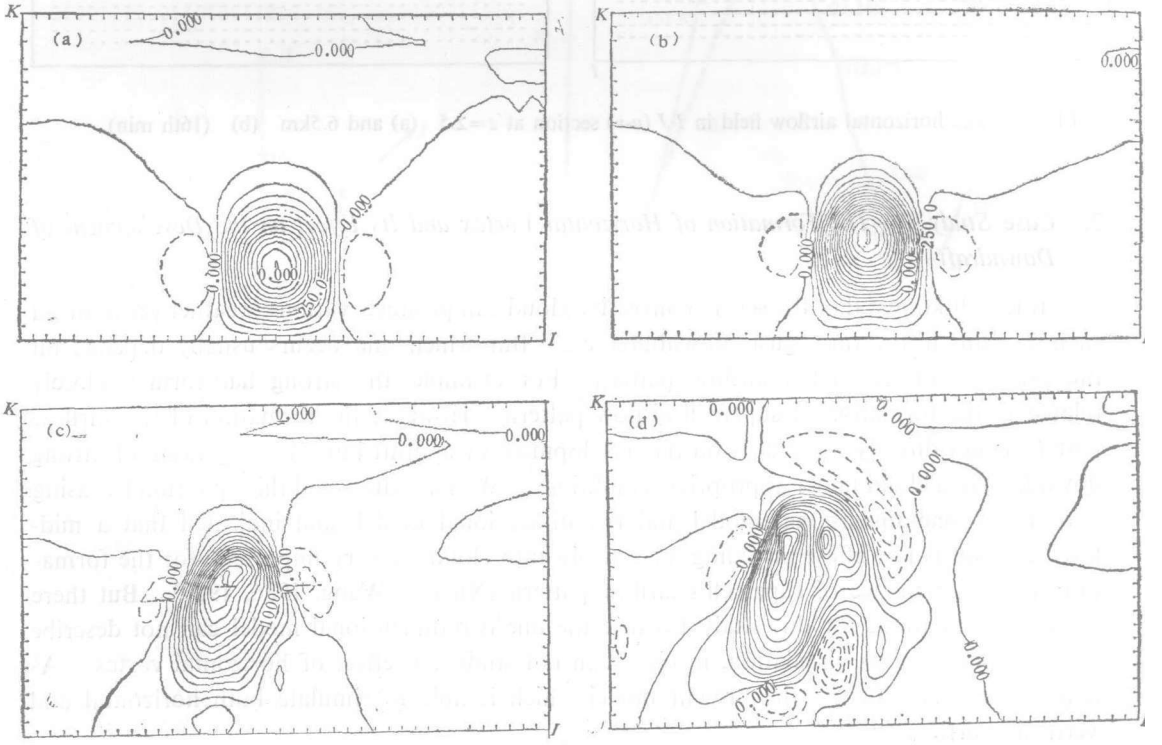

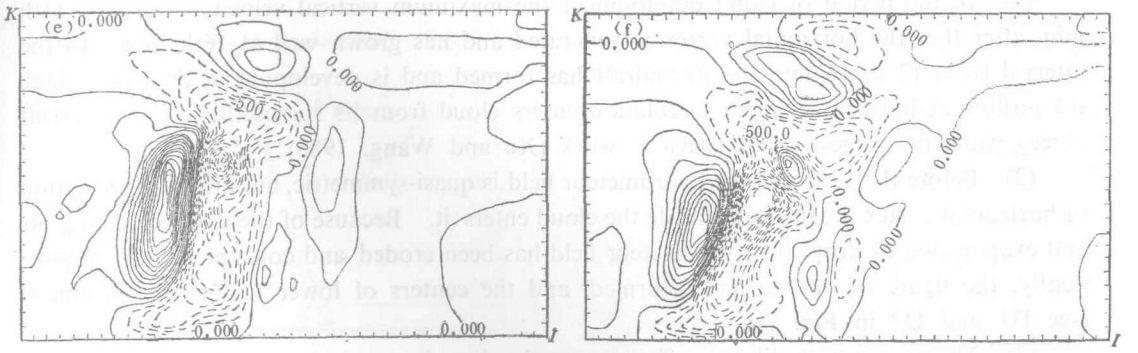

Fig. 5. The section of vertical velocity (solid line stands for updraft and dashed line for downdraft) at $J=20$ and at different times: (a) $T=4$min; (b) $T=8$min; (c) $T=12$min; (d) $T=16$min; (e) $T=20$min; and (f) $T=24$min.

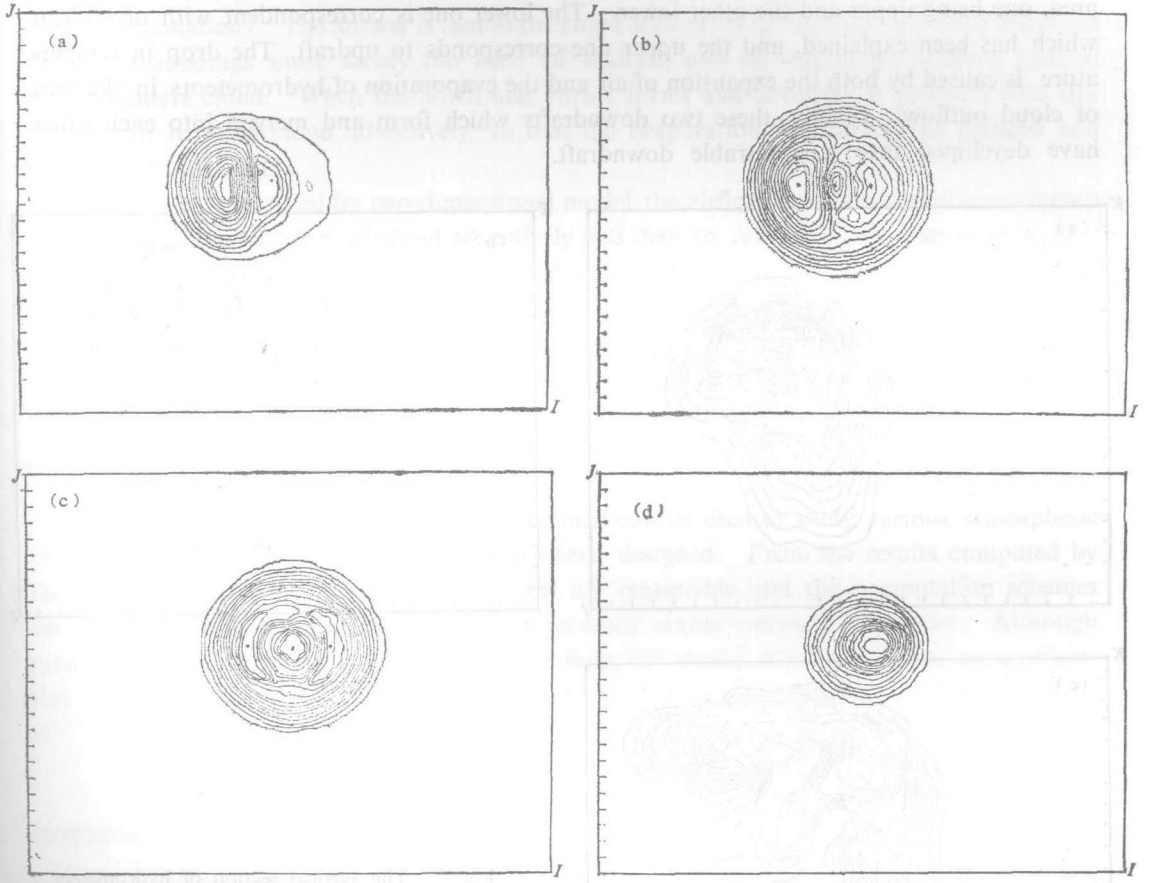

Fig. 6. The horizontal section of hydrometeor field at different levels at 16th min: (a) $z=4.5$km; (b) $z=5.5$km; (c) $z=6.5$km; and (d) $z=7.5$ km.

The results of a case study by GR1 are given in Figs. 3—6. The analysis of these figures shows that:

(1) In the period of cloud development the maximum vertical velocity occurs at 11th min, after that the horizontal vortex is generated and has grown well at 16th min. In the interval from 12 to 16 min the downdraft has formed and is developing in the area where the airflow of horizontal vortex circulation enters cloud from its surroundings. This result agrees with the suggestion of previous work (Xu and Wang, 1986).

(2) Before the 12th min the hydrometeor field is quasi-symmetric, but after the formation of horizontal vortex the dry air outside the cloud enters it. Because of the dilution of vapour and evaporation of drop, the hydrometeor field has been eroded and consumed. Correspondently, the figure of outline has deformed, and the centers of lower value have produced (see D1 and D2 in Fig. 7).

(3) The evaporation-dilution effects cause the drop in temperature, which are very important for inducing and developing downdraft. This process is well seen in Fig. 8. The location of negative disturbance of temperature matches with that of lower value of hydrometeors and downdraft.

From Figs. 3—8 we can also see that there are two negative temperature disturbance area, one being upper and the other lower. The lower one is correspondent with downdraft which has been explained, and the upper one corresponds to updraft. The drop in temperature is caused by both the expansion of air and the evaporation of hydrometeors in the area of cloud outflow. Finally, these two downdrafts which form and merged into each other have developed into a penetrable downdraft.

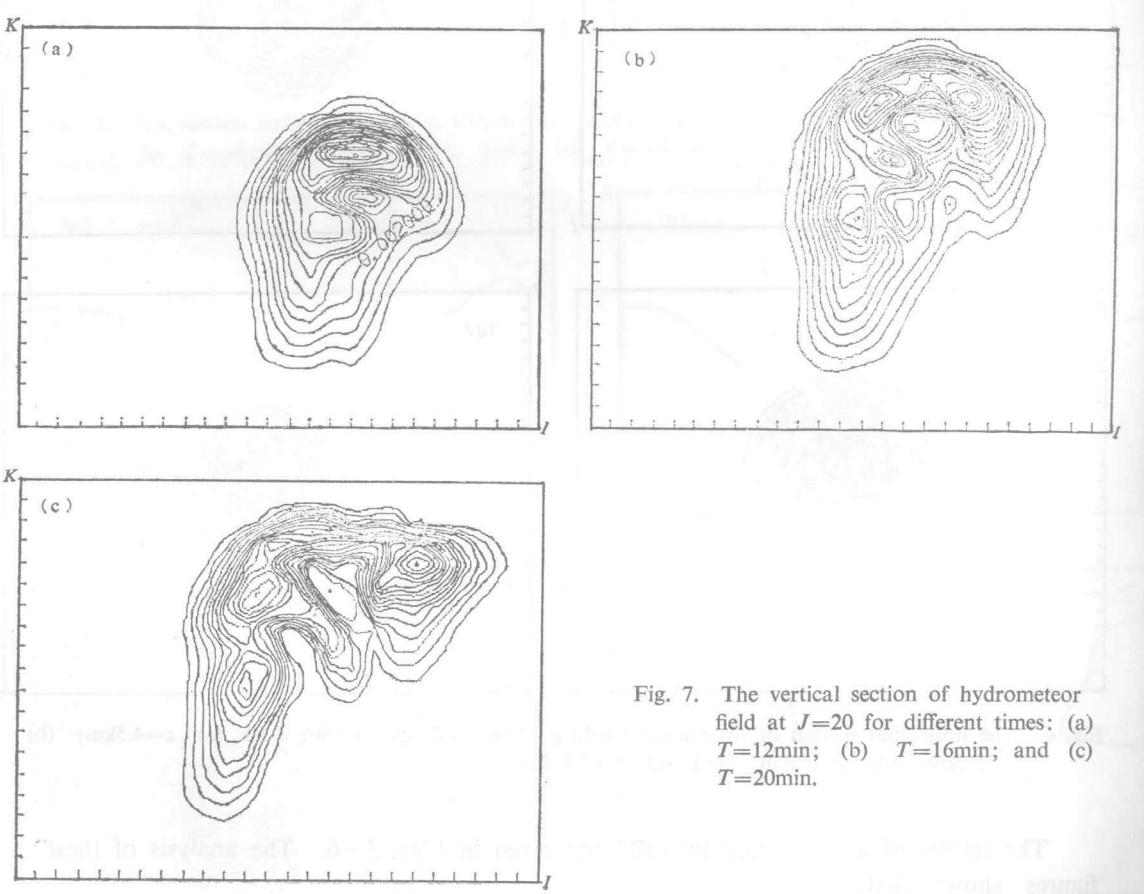

Fig. 7. The vertical section of hydrometeor field at $J=20$ for different times: (a) $T=12$min; (b) $T=16$min; and (c) $T=20$min.

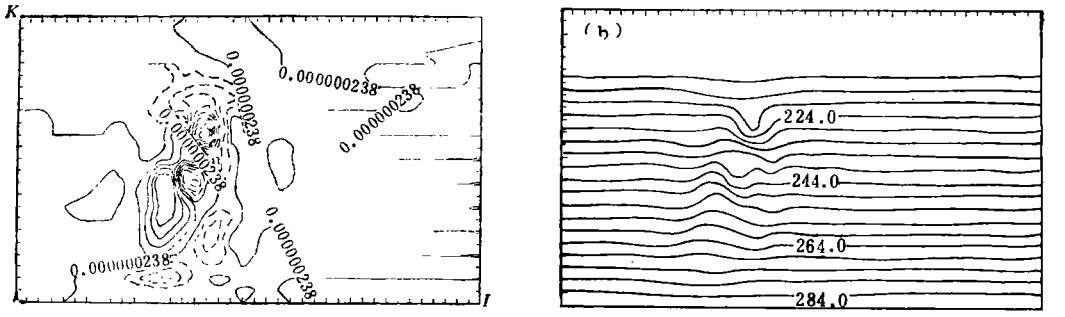

Fig. 8. The section of temperature field (a) and disturbed temperature field (b) at $J=20$ and at 20th min.

V. DISCUSSION

Why the horizontal vortex is more important for the development of downdraft than the vertical circulation? The answer is that in the cloud with updraft, all the air entering the cloud from surroundings must satisfy the need of updraft, and no surplus air without upward motion enters cloud. When the horizontal vortex forms and develops, it provides with dry surplus air to enter cloud advectively, so that the evaporation-dilution can be induced and maintained efficiently.

In the case computed by two-dimensional model the airflow from horizontal convergence is difficult to enter the core of cloud advectively and then to cause the evaporation of hydrometeors. However in three-dimensional model the airflow can run along not only vertical but also horizontal directions so that the air entering the cloud is more than that of two-dimensional model. It may be the reason why the specific content of hydrometeors computed by two-dimensional model is larger than natural when the height of cloud top is consistent.

VI. CONCLUDING REMARKS

Since the three-dimensional cloud-scale model can be used to study various atmospheric phenomena, two versions of the model have been designed. From the results computed by them we can see that the model simulations are reasonable and the computation schemes are stable. The model has a basic function to study severe convective activities. Although running this model needs a lot of computer time, the model can still be run on medium-size computers because the program has a function of restarting and output in batches.

REFERENCES

Anthes, R.A. and Warner, T.T. (1978), Development of hydro-dynamic model suitable for air pollution and other mesometeorological studies, *Mon. Wea. Rev.*, **106**: 1045—1078.

Bates, J.R. and McDonnald, A. (1982), Multiply-upstream, semi-Lagrangian advective schemes: Analysis and application to a multi-level primitive equation model, *Mon. Wea. Rev.*, **110**: 1831—1842.

Chen Shoujun et al. (1980), The brief of a five-level primitive equation model (unpublished).

Klemp, J.B. and Wilhelmson, R.B. (1978), The simulation of three-dimensional convective storm dynamics, *J. Atmos. Sci.*, **34**: 1070—1096.

Schlesinger, R.E. (1975), A three-dimensional numerical model of an isoland deep convective cloud: prelimin-

ary results, *J. Atmos. Sci.*, **32**:934—957.

Tripoil, G.J. and Cotton, W.R. (1982), The CSU three-dimensional cloud/mesoscale model, *J. de Recherches Atmospherigues*, **16**: 185—219.

Xu Huanbin and Wang Siwei (1985a), A numerical model of a hail-bearing convective cloud (1): Bi-parameter evolution of size-distribution of raindrops,frozen raindrops and hailstones, *Acta Meteorologica Sinica*, **43**: 13—25 (in Chinese).

Xu Huanbin and Wang Siwei (1985b), A numerical model of a hail-bearing convective cloud (2): Including bi-parameter size-distribution evolution caused by melting, *Acta Meteorologica Sinica*, **43**: 162—171(in Chinese).

Xu Huanbin and Wang Siwei (1987), A study of two-branch one-dimensional numerical model: Effects of cloud-precipitation development on the formation of vertical circulation in a supercell storm, *Acta Meteorologica Sinica*, **1**:89—95.

Xu Huanbin and Wang Siwei (1989), Two-dimensional numerical hailcloud model, *Acta Meteorologica Sinica*, **3**:200—211.

Zhou Xiaoping et al. (1980), The interpretation of a fine-mesh weather prognostic numerical model (unpublished).